EVAPORATION AND MASS TRANSFER IN WELDING

P. F. MENDEZ*

**Canadian Centre for Welding and Joining, University of Alberta, Canada. Email: pmendez@ualberta.ca*

DOI 10.3217/978-3-99161-089-2-001, license CC BY 4.0

ABSTRACT

This paper reviews the foundations of evaporation and mass transfer in welding operations, presenting for the first time a treatment with simultaneous barriers to mass transfer in the molten metal, at the evaporating surface, and in the surrounding gases. Evaporation is a crucial aspect of welding operations, as it controls fume emissions, arc properties, droplet temperature, porosity, and onset of explosive metal transfer in GMAW of Al-Mg alloys. When evaporation is large a recoil pressure is significant, leading to keyhole penetration in focused beams. The treatment accounts for multicomponent mass transfer, and explicit expressions for the resistance to mass transfer for each component and each stage are provided. A novel treatment for diffusion in the melt is proposed by using an equivalent mass transfer resistance in the melt which allows for the simultaneous consideration of all mass transfer resistances. The treatment of mass transfer also includes a treatment of recoil pressure. The theory is applied to mass transfer and evaporation in the electrode tip in GMAW, with detailed analysis of three experiments with results supporting the theory. Based on the theoretical foundations a criterion for explosive transfer is proposed, reproducing the type and intensity of explosive transfer observed. The treatment presented is also a foundation for a comprehensive formulation of mass and energy balances in deposition rate.

Keywords: Fumes, Metal vapors, mass balance, Energy balance, Recoil pressure

INTRODUCTION

Mass transfer and evaporation in welding have been studied often in the past. There are many motivations for this attention. Evaporation is the source of fumes in welding, which are a topic of much relevance to industrial practice [1], especially Mn and Cr^{6+} components that are often viewed as harmful [2]. Manganese in welding fumes is believed to cause an illness (Manganism) with symptoms similar to Parkinson's disease, and Cr^{6+} is considered a carcinogen. In addition to health considerations, fumes caused by metal evaporation cause productivity losses by required cleaning (e.g. before painting).

Not all effects of evaporation are undesirable, for example selective evaporation during local laser melting of Nitinol shape-memory wires results in changes in transition temperature that can be controlled to design tailor-made components.

An understanding of evaporation is needed for a proper treatment of mass and energy balances [3-4]. In addition to the energy associated with evaporation, there is evidence that evaporation plays a significant role in droplet temperature; for example, although steel has a much higher melting temperature than aluminum, their boiling temperatures are comparable, and so are their droplet temperatures in GMAW. Conversely, the addition of Mg (which has a low boiling temperature) in aluminum wires decreases the droplet temperature. Further analysis of these observations requires an understanding of evaporation.

Metal vapors have a large effect on arc behavior and voltage, with the consequent implications in power source control and waveform design. An understanding of evaporation and the metal vapors surrounding the melt is a necessary step to understand the plasma sheaths around the electrode and plate, especially in the anode.

An understanding of mass transfer is needed to treat the observed behavior of explosive transfer observed in solid wires with high amounts of volatile elements, such as 5XXX aluminum wires.

Despite the strong reasons for understanding mass transfer and evaporation in welding, and despite the amount of attention paid to it, mass transfer in the melt, evaporation, and in the gas have not yet been considered together. In [5], only surface evaporation was considered, while in [6] and [7], only the surface evaporation and gas diffusion are considered, and in [8], only diffusion in the melt is considered.

The treatment in this work is based on the physics of mass transfer with emphasis on the engineering concepts of boundary layer and mass transfer resistance. The mathematical treatment is in the form of engineering expressions such as those used in standard textbooks on heat and mass transfer.

The treatment is general, valid for any alloy and inert shielding gas. Oxidizing shielding gases commonly used in steels such as Ar-2%O_2 or Ar-10% CO_2 are outside the scope of analysis, indeed, even the experiments considered were made with pure Ar. The reason for this limitation is that oxidizing gases react in a way that affects boundary layer thickness, and currently there are no practical expressions for their behavior. The engineering treatment of reactive boundary layers is an exciting area of future work of impact far beyond welding.

The quantitative treatment of boundary layers and mass transfer resistances leverages on the mathematical analogy between fluid flow, heat transfer, and mass transfer, such that advanced expressions for mass transfer can be postulated based on extensive studies of heat transfer, of which the literature is much more abundant.

In all cases, the expressions verified in practice were never accurate than ±20% considering uncertainty in the physics, configurations, and fluid properties. In this work, the sign "=" is used in almost all equations for simplicity instead of "≈", with the understanding that the existing expressions used and the new expressions derived are far from mathematical equalities.

In this work three experiments are considered which are representative of a larger set of experiments performed in the past. The goal of the experiments chosen is to be illustrative, as a proper validation of the foundations presented here will require a few theoretical extensions

listed in the Discussion section, as well of simultaneous measurements that although possible, have never been performed before, such as simultaneous droplet temperature measurements and fume characterization. Similarly, the theory developed has been applied as a case study only to the electrode tip in GMAW, but other applications such as evaporation from the weld pool in GTAW or power beams in conduction mode could readily be considered.

The ultimate goal of this work is on setting a foundation for future modeling and experimental work with a higher level of understanding of the physical mechanisms involved and interplay of process parameters.

FUNDAMENTALS OF MASS TRANSFER

THE CONCEPT RESISTANCE TO MASS TRANSFER

The concept of resistance to mass transfer ($\Re$) is an analog of electrical resistance, but it is associated with the steady or quasi-steady mass transfer $\dot{m}$ between two points A and B in the same phase. It is defined in this work as

$$\Re = \frac{c_{\mathrm{A}} - c_{\mathrm{B}}}{\dot{N}} \tag{1}$$

where c_A and c_B correspond to the concentrations of solute in the phase considered in mol m^{-3}, and N is the molar flow from point A to point B.

This definition assumes that the chemical potential of the solute in the phase considered is proportional to its concentration. This consideration, it is not directly applicable to the case when points A and B are in different phases such as liquid and gas. When multicomponent mass transfer is considered (e.g. simultaneous mass transfer of Fe and Mn), the component considered is indicated in the subscript, e.g. $\Re_{\mathrm{Fe}}$, $\dot{N}_{\mathrm{Fe}}$. The definition of $\Re$ stays the same if concentration and flow involve units of mass instead of mol.

When mass transport happens in the gas phase, considering the gases and vapors as ideal gases:

$$c_j = \frac{p_j}{RT} \tag{2}$$

where c_j is the concentration of a vapor component j, p_j is its partial pressure, and T its temperature, resulting in

$$\Re_j = \frac{p_{A\,j} - p_{B\,j}}{RT\dot{N}_j} \tag{3}$$

where p_{A_j} and p_{B_j} are the partial pressures of the vapor component j at points A and B, both at the same temperature T. The effects of temperature gradients on mass transport in gases are not considered in this work, but future work should incorporate them.

Resistances in series One convenient feature of the concept of resistance to mass transfer is that it can tackle with efficiency problems with multiple mass transfer mechanisms. In particular, when the mass transfer mechanisms are sequential, the problem can be modeled as a set of resistance in series.

$$\Re_{\mathrm{tot}_j} = \Re_{1_j} + \Re_{2_j} \tag{4}$$

where $\Re_{\mathrm{tot}_j}$ is the total resistance to mass transfer for component *j*, $\Re_{1_j}$ and $\Re_{2_j}$ are two resistors in series. The applicability of this equation is limited to resistances to mass transfer *in the same phase*. The reason is that the driving force for diffusion is different if a concentration gradient is in one phase (e.g. molten metal) or another (e.g. gas phase).

Under some conditions, it is possible to define an ``equivalent' resistance to mass transfer that takes into account the different phases.

Dominant resistance The value of resistances to mass transfer might be different by an order of magnitude or more. When multiple resistances to mass transfer are in series, if a resistance is much smaller than the others, it can be neglected to simplify calculations; if a resistance is much larger than the sum of all others, it can be considered dominant and all other resistances can be neglected. When the largest resistances are of comparable magnitude, they are in an intermediate regime where none is dominant; for example, in the electrode tip in GMAW of Al-Mg alloys, the resistance to mass loss of aluminum is typically dominated by the gas phase, while for Mg, the resistance of evaporation is negligible and the resistances in the melt and in the gas are comparable.

Resistance per unit area An important concept associated with mass transfer resistance is that of ``resistance associated with a unit area " $\Re$'':

$$\Re_j'' = \frac{c_{A_j} - c_{B_j}}{J_j} \tag{5}$$

where J_j is the molar flow per unit area (mol s^{-1} m^{-2}) of component *j*. This concept is useful when mass transfer happens over an extended area, such as evaporation at the surface of the molten electrode or the molten weld pool.

Typical values of $\Re_j''$ at the electrode tip in GMAW are of the order of 10^3 s m^{-1} for Mn in molten steel wires, 10^2 s m^{-1} for Mg in molten aluminum, and 10^{-1} s m^{-1} for metal vapors in Ar of the shielding gas. If a resistance per unit area is obtained, a flux can be calculated as

$$J_j = \frac{c_{A_j} - c_{B_j}}{\Re_j''} \tag{6}$$

with its analog for gases:

$$J_j = \frac{p_{A_j} - p_{B_j}}{RT\Re_j''} \tag{7}$$

For an area *A* of constant flux:

$$\Re_j'' = A\Re_j \tag{8}$$

and for an area A over which the flux varies, an average resistance to mass transfer is defined as

$$\overline{\Re''_j} = A\Re_j \tag{9}$$

Note that the magnitude A is multiplied, not divided as would be expected in a quantity associated with a unit area. A mass flux $\dot{m}''$ in kg s^{-1} m^{-2} is related to the molar flux as

$$\dot{m}''_j = M_j J_j \tag{10}$$

where M_j is molar mass of component j in kg mol^{-1}. A total mass transfer can be obtained as

$$\dot{m}_j = AM_j\bar{J}_j \tag{11}$$

where $\bar{J}_j$ is the surface average flux over area A. The amount of mass evaporated from the tip of a GMAW electrode is of the order of 1% of the electrode mass.

MECHANISMS OF MASS TRANSFER

Resistances to mass transfer can be associated with different mechanisms. The application of these mechanisms together with the concept of boundary layer result in practical expressions to evaluate mass transfer in welding. These expressions are approximate even under the idealized conditions in which they were developed, with an accuracy not better than 20% [9]. Natural convection is typically negligible for both molten metal [6], shielding gas, and vapors [10] in the active part of welding (around the weld pool and molten consumable). The temperature of a gas evaporating from a free surface at temperature T_s is slightly lower than T_s, but they will be assumed to be the same for simplicity.

Diffusion

Diffusion for component j is associated with Fick's law. When diffusivity is constant:

$$\Re_{\text{diff}_j} = \frac{1}{S_j D_j} \tag{12}$$

where S is the "shape factor" associated with a given geometry. Shape factors are tabulated for many ideal geometries [9]. For a sphere of radius a in an infinite medium $S=4\pi a$, and for the case of uniform diffusion across a layer of surface area A and thickness $\eth$, such as the gas boundary layer on the free surface of molten metal at the electrode or weld pool, $S=A/\eth$ where $\eth$ is the thickness of the layer, resulting in

$$\Re_{\text{diff, layer}_j} = \frac{\eth}{AD_j} \tag{13}$$

and its equivalent associated with a unit area

$$\Re''_{\text{diff, layer}_j} = \frac{\mathfrak{d}}{D_j} \tag{14}$$

When diffusivity varies across the thickness of the layer, an effective value of diffusivity is proposed in Appendix A. Parameters for the calculation of diffusivity of components in molten steel and aluminum are given in Appendix B, and of metal vapors in shielding gases in Appendix C

Advection

Advection is the transport of a quantity by the motion of matter. For a given surface of a control volume, advection of a solute across a control surface is

$$J_{\text{adv}_j} = c_j u_j \tag{15}$$

where c_j is the concentration of solute component j and u is the component of velocity perpendicular to the surface of the control volume. the velocity u is a velocity in the molten metal, gas, or vapor.
For vapors exiting the surface during evaporation, if the vapors are treated as an ideal gas and the volume of liquid or solid is neglected:

$$u_j = J_{\text{adv}_j} \frac{RT_s}{p_{s_j}} \tag{16}$$

where $u_j$is the velocity of vapor component j exiting the surface in a direction perpendicular to it, J_{adv_j} is the molar flow of vapor component j, T_s is the temperature of the evaporating surface, and p_{s_j} is the partial pressure of vapor component j just outside the surface. Of course, this equation is valid for subsonic velocities and pressures high enough for an ideal gas behavior.

Convection

The combination of diffusion and advection in fluids results in convection. Across an interface in which one side is a fluid, viscous, thermal, and diffusion boundary layers establish on the fluid side (this applies to both sides on a fluid-fluid interphase such as shielding gas over molten metal). Convective mass transport into the fluid happens by diffusion across the diffusion boundary layer, and can be quantified as

$$J_{\text{conv}_j} = \mathfrak{h}_j \left(c_{s_j} - c_{\infty_j} \right) \tag{17}$$

where c_{s_j} and c_{∞_j} are the concentrations of component j in the fluid near the surface and just outside the boundary layer. The units of $\mathfrak{h}_j$are m s^{-1}. Typical values of $\mathfrak{h}_j$ at the electrode tip in GMAW are of the order of 10^{-3} m s^{-1} for Mn in molten steel wires, 10^{-2} m s^{-1} for Mg in

molten aluminum, and 10^1 m s^{-1} for metal vapors in Ar of the shielding gas. The mass transfer resistance of convection is obtained by applying the definition of thermal resistance (Equation 5) to Equation 17, resulting in

$$\Re''_{\text{conv}\,j} = \frac{1}{\mathfrak{h}_j} \tag{18}$$

Evaporation

Evaporation from a surface is typically described as [11]

$$J_{e\,j} = \beta_j \frac{p_{\text{l,s}\,j} - p_{\text{g,s}\,j}}{\sqrt{2\pi M_j R T_s}} \tag{19}$$

where $p_{\text{l,s}\,j}$ is the vapor pressure of component j in the melt at the free surface, and $p_{\text{g,s}\,j}$ is the pressure of the metal vapor in the gas right at the free surface and β_j is the coefficient of evaporation and condensation for component j, always below 1, but close to it [11]. Considering the gas as ideal, Equation 2 can be applied to the definition of resistance to mass transfer (Equation 1) resulting in the following mass transfer resistance for evaporation:

$$\Re''_{\text{e}\,j} = \frac{1}{\beta_j}\sqrt{\frac{2\pi M_j}{R T_s}} \tag{20}$$

Although Equation 20 involves both the liquid and gas phases, it is based on the concentrations in the gas phase. If Mn is evaporating from an ER70S steel GMAW electrode (approximately 1 wt% Mn), the concentration used with this mass transfer resistance is not the molar volume of 1 wt% Mn in the molten steel, but instead the much larger molar volume of 1 wt% Mn as a vapor at the temperature of the free surface and corresponding vapor pressure or partial pressure. The resistance associated with evaporation is typically negligible at the electrode tip in GMAW.

Multicomponent evaporation In multicomponent evaporation, the partial vapor pressure of component *j* in the melt is proportional to the activity in the alloy [5]

$$p_{\text{l}\,j} = a_j p_{\text{lg}\,j} \tag{21}$$

where $p_{lg\,j}$ is the equilibrium vapor pressure of element j in pure state. In this case, we will approximate the activity$a_j$using Raoult's law:

$$a_j = X_j \tag{22}$$

where X_j is the molar fraction of j on the evaporating surface.

$$X_j = \frac{c_j M}{\rho} \tag{23}$$

with ρ being the density and M the overall molar mass of the melt

$$M = \left(\sum_j \frac{f_j}{M_j} \right)^{-1} \tag{24}$$

with f_j the mass fraction of component j in the melt. Parameters to calculate vapor pressure are tabulated in Appendix D. Conversion formulae for mass and molar fractions are listed in Appendix E. The overall density and molar mass M are typically very close to those of the main alloy component, such as aluminum or iron.

Effective diffusion resistance in the melt Equations 21-23 indicate that composition variations in the melt could be expressed in terms of the vapor pressures associated with each composition.

$$\Delta c_{\mathrm{l}_j} = \frac{\rho}{p_{\mathrm{lg}_j} M} \Delta p_{\mathrm{l}_j} \tag{25}$$

where ρ and p_{lg_j} are taken at the temperature of the free surface. Replacing the concentration difference in Equation 6, we obtain

$$J_j = \frac{\rho}{M p_{\mathrm{lg}_j} \Re''_{l\,j}} \Delta p_{\mathrm{l}_j} \tag{26}$$

Comparing Equation 26 with Equation 7, we can define an equivalent resistance for diffusion in the melt $\Re''_{\mathrm{l,eq}_j}$ that can be used in the reference frame of metal vapors

$$\Re''_{\mathrm{l,eq}_j} = \frac{p_{\mathrm{lg}_j} M}{\rho R T_s} \Re''_{\mathrm{l}\,j} \tag{27}$$

The conversion factor in Equation 27 is of the order of 10^{-2} for Mg in Al and 10^{-4} for Mn in steel in the cases considered.

Recoil pressure Conservation of momentum indicates that the mass evaporated causes a pressure (``recoil pressure") on the free surface from where it originates. Recoil pressure has been studied in insufficient detail in the past because it requires an understanding of mass flow affected by boundary layers in the liquid and gas phases, as well as evaporation. In [12], the recoil pressure is obtained with electromagnetic arguments alone, while in [13], a recoil pressure is calculated neglecting the heat conducted into the substrate and without accounting for resistance to mass transfer. In [14], the recoil pressure is calculated semi-empirically without accounting for mass transfer mechanisms that dominate the rate of evaporation.

The recoil pressure is in addition to the partial pressure of the vapor. At high surface temperatures, the rate of evaporation is fast and the recoil pressure is significant, for example recoil pressure is the cause of a keyhole in power beam welding. The total recoil pressure is given by the addition of the recoil pressures of each evaporating component

$$p_{\mathrm{rec}\,j} = \dot{m}''_j u_j \tag{28}$$

where $\dot{m}''_j$ is the rate of mass of component *j* evaporated (Equation 10) and u_j is the velocity of the vapors exiting the surface (Equation 16), resulting in

$$p_{\mathrm{rec}_j} = {J_j}^2 \frac{M_j R T_s}{p_{\mathrm{g,s}_j}} \tag{29}$$

where p_{s_j} is the partial pressure of component *j* at the surface, always higher than the recoil pressure, such that

$$p_{\mathrm{g,s}_j} = p_{\mathrm{rec}_j} + p_{\mathrm{diff}_j} \tag{30}$$

with p_{diff_j} being the partial pressure of component *j* at the surface when considering only diffusion in the gas boundary layer $\Re''_{\mathrm{g}_j}$. Using Equation 7 with a metal vapor pressure of zero away from the boundary layer:

$$p_{\mathrm{diff}_j} = R T_{\mathrm{s}} \Re''_{\mathrm{g}_j} J_j \tag{31}$$

Equations 30 and 31 can be combined to solve for J_j, and this flux can be used into Equation 29 resulting in the following equation

$$\frac{p_{\mathrm{rec}_j}}{p_{\mathrm{g,s}_j}} = \left(1 - \frac{p_{\mathrm{rec}_j}}{p_{\mathrm{g,s}_j}}\right)^2 \frac{M_j}{R T_s {\Re''_g}_j^{\,2}} \tag{32}$$

where it can be seen that when the resistance to mass transfer in the gas boundary layer is significant, the recoil pressure is small and can be calculated as

$$p_{\mathrm{rec}_j} = \frac{M_j J_j}{\Re''_{\mathrm{g}_j}} \quad \text{for } p_{\mathrm{rec}_j} \ll p_{\mathrm{g,s}_j} \tag{33}$$

and conversely, if the ratio of mass flow to resistance to mass transfer in the gas boundary layer is large, the recoil pressure dominates the gas pressure on the surface, and $p_{g,s_j} = p_{rec_j}$. In all experiments considered, this was the case, with the recoil pressure being at least 700 times the diffusion pressure. In this case, Equation 29 results in

$$p_{\mathrm{rec}_j} = J_j \sqrt{M_j R T_s} \quad \text{for } p_{\mathrm{rec}_j} \approx p_{\mathrm{g,s}_j} \tag{34}$$

and if the overall dominant resistance to mass transfer is that of evaporation, for example in the evaporation of the main alloy component in vacuum during EBW, incorporating Equation 19, with p_{s_j} results in

$$p_{\mathrm{rec}_j} = \frac{p_{\mathrm{l,s}_j}}{\sqrt{2\pi}/\beta_j + 1} \approx \frac{p_{\mathrm{l,s}_j}}{3.5} \tag{35}$$

This equation gives the maximum possible recoil pressure. The evaporation of pure metals in vacuum was also studied in [15]. Additional mass transfer resistances such as diffusion in the

melt or in the gas will yield lower recoil pressures. For the GMAW cases studied, the recoil pressure was of the order of 10^2-10^3 Pa, much higher than the pressure associated with diffusion (Equation 34), but comparable with the arc pressure at the droplet [16], of a magnitude that could potentially lift the molten droplet.

Heat loss by evaporation Evaporating components take away their latent heat as they evaporate. The thermal energy associated with each component is

$$q''_{\mathrm{v}\,j} = \dot{m}''_{\mathrm{v}\,j}\, i_{\mathrm{lg}_j} \tag{36}$$

where $\dot{m}''_{v\,j}$ is the amount of component *j* evaporated (Equation 10) and i_{lg_j} is the enthalpy of evaporation of component *j*. The energy balance due to evaporation has been studied in detail in [17], being of the order of 10^2 W, or approximately 1% of the whole energy balance for the GMAW experiments performed.

BOUNDARY LAYERS

Boundary layers are thin regions in a fluid parallel to an interphase, for example in the gas phase surrounding the free surface of molten metal, or in the molten metal just under the free surface. This thin layer contains the significant part of the gradient driving the mass transfer across the interphase.

The concept of boundary layer is valid when it is thin compared to the dimensions of the object being considered. For the case of gases surrounding the molten consumable or the weld pool, the boundary layers need to be much thinner than the characteristic length of the weld pool or molten consumable; for the case of molten metal, the boundary layer needs to be much thinner than the depth of the weld pool or the size of molten consumable.

Three types of boundary layers are relevant in this work: viscous, thermal, and diffusion. There are multiple diffusion boundary layers: one per solute component; for example, in the 5183 aluminum filler metal, there is a diffusion boundary layer for Mg with thickness $ð_{\mathrm{Mg}}$, and another one for Mn with thickness $ð_{\mathrm{Mn}}$, plus additional boundary layers for minor elements.

In this analysis, it is assumed that the solute is relatively dilute in the solvent. This is applicable to steel alloys with approximately 1 wt% of Mn as the volatile component and aluminum alloys which typically contain less than 5 wt% Mg as their volatile component. This hypothesis is not properly fulfilled on occasions in the gas phase when the solute evaporates much more than the solvent. This hypothesis is not appropriate also in multi-princial component alloys. Further work is needed to improve this work under those conditions. An important consequence of considering dilute solutions is that their density can be treated as independent of their composition.

Another consideration in this paper is that of non-reactive boundary layers, i.e., we consider only evaporation in an inert atmosphere such as GMAW of aluminum alloys using pure Ar shielding, and apply the results even in cases of reactive boundary layer such as in GMAW of steel alloys using Ar-O_2 or Ar-CO_2 shielding. It is known that the reaction reduces the thickness of the boundary layer, resulting in increased evaporation [18-19] and fumes

formation [20] [21]. The association of carbon with oxygen on the surface of the melt can result in decarburization of the melt.

The concept of boundary layer is taken as a good approximation for the case in which the vapor pressure approaches atmospheric pressure. Also, motion at the interphase, such as surface flow velocity of the free surface on a liquid/gas interphase, or velocity caused by the melting or evaporation of the interphase are neglected. These velocities at the interphase are typically negligible when compared to the velocity outside the boundary layer of the fluid in question.

Diffusion boundary layer When the diffusivity is constant across the boundary layer (or an effective value is used), the coefficient of mass convection for component *j* relates to the thickness of the diffusion boundary layer as

$$\mathfrak{h}_j = \frac{D_j}{\mathfrak{d}_j} \tag{37}$$

where the thickness of the diffusion boundary layer is defined as

$$\mathfrak{d}_j = \frac{c_{s\,j} - c_{\infty\,j}}{dc_j/dy\,|_s} \tag{38}$$

where $dc_j/dy\,|_s$ is the concentration gradient in the fluid at the interphase. Typical values of diffusion boundary layer thickness at the GMAW electrode tip are 10-100 μm in the melt and 300 μm in the gas phase, both much thinner than the droplet diameter of about 2 mm. The thickness of the diffusion boundary layer is seldom calculated using the definition of Equation 38, so the differential expression seldom needs to be evaluated.

Viscous boundary layer The thickness of the related viscous boundary layer is defined in this work as

$$d = \frac{u_\infty}{du/dy|_\mathrm{s}} \tag{39}$$

where u_∞ is the velocity of the fluid just outside the boundary layer and $du/dy|_\mathrm{s}$ is the velocity gradient in the fluid at the interphase. This definition neglects the velocity of the interphase, such as the surface velocity of the molten metal in the weld pool when calculating the boundary layer of gases on the surface of the weld pool.

Thermal boundary layer The definition of the thermal boundary layer is

$$\ell = \frac{T_\mathrm{s} - T_\infty}{dT/dy|_\mathrm{s}} \tag{40}$$

where T_s and T_∞ are the temperature of the fluid at the surface and just outside the boundary layer and $dT/dy|_\mathrm{s}$is the temperature gradient in the fluid at the interphase. The associated convection coefficient for heat transfer is

$$h = \frac{k}{\ell} \tag{41}$$

where *k* is the thermal conductivity of the fluid.

Tabulation of convection coefficients in boundary layers The diffusion convection coefficient for each component is tabulated in dimensionless form as the Sherwood number based on a characteristic length *L*.

$$\mathrm{Sh}_j = \frac{\mathfrak{h}_j L}{D_j} = \frac{L}{\mathfrak{d}_j} \tag{42}$$

where the second equality results from application of Equation 37. The thermal convection coefficient is tabulated in dimensionless form as the Nusselt number based on a characteristic length *L*.

$$\mathrm{Nu} = \frac{hL}{k} = \frac{L}{\ell} \tag{43}$$

where the second equality results from application of Equation 41. A mass transfer resistance for the diffusion boundary layer can be obtained from the Sherwood number as

$$\mathfrak{R}_j'' = \frac{L}{D_j \mathrm{Sh}_j} \tag{44}$$

In the laminar case, the average convection coefficients $\overline{h}$, $\overline{\mathfrak{h}}_j$, average Nusselt $\overline{\mathrm{Nu}}$ or average Sherwood $\overline{\mathrm{Sh}}_j$ between *x=0* and *x=L* are $\overline{h}$=*2h*, $\overline{\mathfrak{h}_j}$, $\overline{\mathrm{Nu}}$=2Nu, and $\overline{\mathrm{Sh}}_j$=2Sh$_j$ where *h*, Nu, and Sh$_j$ are local values at *x=L*.

The notation $\overline{\mathfrak{R}_j}$ will indicate a mass transfer resistance calculated with an average Sherwood number ($\overline{Sh_j}$), it is not a mathematical average; however, when integrating mass flux over a surface of area A, because of the parallel nature of mass transfer on each element of surface, it can be stated with mathematical rigor that

$$\mathfrak{R}_j = \frac{AL}{D_j \overline{\mathrm{Sh}}_j} \tag{45}$$

where $\overline{\mathrm{Sh}}_j$ is typically considered that over a flat surface. More accurate calculations are possible for geometries other than a flat surface, but the increase of precision does not justify the increase in complexity in the context of the large uncertainties of the expressions used and the properties of fluids considered.

Hypotheses of boundary layer theory Boundary layer theory is based on a number of simplifications that are usually representative of reality. Three key considerations are included here.

The boundary layer is thin compared to the geometry considered: Both $\overline{Sh_j}$ and Nu must be much greater than 1 because the thickness of the boundary layer thickness should be much smaller than the characteristic length. When their value approaches 1, the problem becomes one of static diffusion or conduction heat transfer, not convection.

The flow outside the boundary layer is advection dominated: The Peclet number must be much greater than 1. The Peclet number is a metric of the dominance of advection, and is defined based on the length of the boundary layer *x* as

$$\mathfrak{Pe}_j = \frac{u_\infty x}{D_j} \tag{46}$$

In the experiments considered, the Peclet number was always greater than 10^2 in the melt and greater than 30 in the gas.

The boundary layer is in quasi-steady state; this implies the hypothesis that the fluid flow is also in quasi-steady state and there was enough time to develop the boundary layer.
A time scale for fluid dynamics can be estimated as

$$t_u = \frac{L}{u} \tag{47}$$

where L is the characteristic length of the flow, and u is the characteristic velocity of the flow. A timescale for the formation of a boundary layer is given by

$$t_{\mathfrak{d}_j} = 0.5\frac{{\mathfrak{d}_j}^2}{D_j} \tag{48}$$

If both t_u and $t_{\mathfrak{d}_j}$ are shorter than the droplet detachment period or waveform times, mass transfer can be approximated as steady-state. For the cases of GMAW studied, $t_u \approx 4$ ms and $t_{\mathfrak{d}_j} \approx 7$ ms, approximately 30% of the droplet detachment time.

Boundary layer with shear

When the interphase separates a fluid (molten metal or gas) from a solid (or a static liquid), three types of boundary layers are established: viscous, thermal, and diffusion. The thickness of the viscous boundary layer is relatively independent from the other two and is associated with shear over a solid or liquid surface. The thicknesses of the thermal and diffusion boundary layers depend on the viscous one.

In welding, the motion of gases and molten metal is typically laminar, and this will be the focus of this boundary layer treatment. Some welding processes such as electroslag (ESW) and electrogas (EGW) might involve turbulence. The modeling of the arc in other arc welding processes such as GTAW [10], GMAW, and power beam processes such as laser (LBW) and electron beam (EBW) has traditionally been as laminar flows. There are indications that the weld pool might involve turbulence [22].

Because boundary layers are thin compared to the size of the weld pool or the molten 10^1able, f10^3 quantitative analysis of this section they will be considered as if they were over a flat surface, for which accurate expressions exist [9, 23].

Viscous boundary layer with shear Using the definition of Equation 39, the thickness of the viscous boundary layer over a flat plate is

$$d = 3\sqrt{\frac{\nu x}{u_\infty}} \tag{49}$$

where ν is the kinematic viscosity of the fluid. An effective value of kinematic viscosity is proposed in Appendix A, and temperature-dependent properties for steel and aluminum are in Appendix B. The coordinate x is defined along the interphase in the direction of the flow with $x=0$ corresponding to the moment the flow starts on the interphase, e.g. the edge of the anode spot on the tip of GMAW electrode of positive polarity, which will be discussed in detail below.

For comparison, the commonly used definition of viscous boundary layer thickness as that where the velocity is 99% of that of the external flow results in a factor of 5 instead of 3 in Equation 49. The concept of viscous boundary layer is valid only when Re $\gg$1. Re is the Reynolds number defined as

$$\mathrm{Re} = \frac{u_\infty x}{\nu} \tag{50}$$

Thermal boundary layer with shear The thickness of the thermal boundary in the presence of a viscous boundary layer is

$$\ell \approx \begin{cases} \sqrt{\pi}\sqrt{\dfrac{\nu x}{u_\infty}}\,\mathrm{Pr}^{-1/2} & \text{for } \mathrm{Pr} \ll 1 \\ 3\sqrt{\dfrac{\nu x}{u_\infty}}\,\mathrm{Pr}^{-1/3} & \text{for } \mathrm{Pr} \gtrsim 1 \end{cases} \tag{51}$$

where Pr is the Prandtl number, defined as

$$\mathrm{Pr} = \frac{\nu}{\alpha} \tag{52}$$

with α being the thermal diffusivity. The concept of thermal boundary layer is valid only when Pe $\gg$ 1. Pe is the Peclet number defined as

$$\mathrm{Pe} = \frac{u_\infty x}{\alpha} \tag{53}$$

When using effective values, an effective value for α is proposed in [24]. In molten metals, the value of Pr is typically much less than 1 and in gases is approximately 1, suggesting that the exponent to use in Equation 51 is -1/3. In plasmas Pr is often much less than 1. and the exponent would be -1/2.

A consequence of the value of Pr near or below 1 is that in molten metals and plasmas, the thermal boundary layer is larger than the viscous boundary layer, while for gases the values are comparable. In all cases, the temperature gradient in the viscous boundary layer can be considered approximately linear, making Equation 87 applicable.

Combining equations 41, 51, and 43, a dimensionless expression for thermal convection across a laminar boundary layer with shear is

$$\mathrm{Nu} \approx \begin{cases} \frac{1}{\sqrt{\pi}} \mathrm{Re}^{1/2} \mathrm{Pr}^{1/2} & \text{for } \mathrm{Pr} \ll 1 \\ \frac{1}{3} \mathrm{Re}^{1/2} \mathrm{Pr}^{1/3} & \text{for } \mathrm{Pr} \gtrsim 1 \end{cases} \tag{54}$$

Diffusion boundary layer with shear The thickness of the diffusion boundary for each component in the presence of a viscous boundary layer is

$$\mathfrak{d}_j \approx \begin{cases} \sqrt{\pi} \sqrt{\frac{\nu x}{u_\infty}} \mathrm{Sc}_j^{-1/2} & \text{for } \mathrm{Sc}_j \ll 1 \\ 3 \sqrt{\frac{\nu x}{u_\infty}} \mathrm{Sc}_j^{-1/3} & \text{for } \mathrm{Sc}_j \gtrsim 1 \end{cases} \tag{55}$$

where Sc_j is the Schmidt number, for component j defined as

$$\mathrm{Sc}_j = \frac{\nu}{D_j} \tag{56}$$

In gases, Sc_j is approximately 1, suggesting that the exponent to use in Equation 55 is -1/3. A consequence of the value of Sc_j is that in gases the diffusion boundary layer is smaller than the viscous boundary layer. Plasma diffusivity values are not surveyed in this work, but are expected to have a Sc_j number comparable to gases. Detailed analysis of diffusion in plasmas is in [25 - 27]. In molten metals, the diffusion boundary layer is typically thinner than the thermal boundary layer and in gases it is comparable or thinner. In molten metals, the value of Sc_j can be larger or smaller than one.

Combining equations 37, 55 and 42, a dimensionless expression for mass convection across a laminar boundary layer with shear is

$$\mathrm{Sh}_j \approx \begin{cases} \frac{1}{\sqrt{\pi}} \mathrm{Re}^{1/2} \mathrm{Sc}_j{}^{1/2} & \text{for } \mathrm{Sc}_j \ll 1 \\ \frac{1}{3} \mathrm{Re}^{1/2} \mathrm{Sc}_j{}^{1/3} & \text{for } \mathrm{Sc}_j \gtrsim 1 \end{cases} \tag{57}$$

Boundary layer without shear

At the free surface of the weld pool or at the free surface of the molten consumable, the molten metal is moving, but it is not in contact with a solid that could impose shear forces. In these cases, there is no viscous boundary layer; however, thermal and diffusion boundary layers still exist.

In the absence of shear, there are no steep gradients near the free surface of the molten metal, and this molten metal can be treated as a solid. When the Peclet number (thermal or diffusion) is much larger than 1, conduction and diffusion are essentially 1D processes across

the thickness of the boundary layer, and solutions for a semi-infinite solid such as those in [9] can be applied.

In the absence of shear, the results of equations 51, 55, 54, 57 corresponding to low Pr or low Sc_j apply to *all* values of Pr or Sc, i.e. the expressions with exponent of 1/2 for Pr or Sc_j apply to all cases.

Mass transfer from a sphere

The treatment of boundary layers indicates that an analogy between heat and mass transfer is possible by replacing Pr by Sc_j and Nu by Sh_j in theoretical or empirical correlations. In addition to the correlations for boundary layer described above, there is a good wealth of empirical correlations for heat transfer for $\mathrm{Pr} \gtrsim 1$ (typical of air, water, and oil) that can be adapted for mass transfer where $\mathrm{Sc}_j \gtrsim 1$ in all relevant cases.

Mass transfer from a sphere of radius a immersed in a fluid of velocity u_∞ can be estimated using the following expression [9]

$$\overline{\mathrm{Sh}_j} = 2 + 0.6\,\mathrm{Re}^{1/2}\mathrm{Sc}_j{}^{1/3} \tag{58}$$

where the Reynolds number is evaluated using the diameter $2a$ as a reference length and the velocity considered is u_∞. The value of 2 corresponds to pure diffusion without advection using the shape factor for a sphere. This equation is an approximation bridging between pure diffusion ($\mathrm{Re} \to 0$) and pure convection ($\mathrm{Re} \gg 1$) using traditional blending [28] with n=1. If not using effective values, practical fluid properties are obtained at the "film temperature" intermediate between the surface temperature and the fluid temperature.

MASS TRANSFER AT THE ELECTRODE TIP IN GMAW

The geometry of the electrode tip varies with time, and this causes the resistances to heat and mass transfer to vary with time. In addition, the local resistances also vary as the geometry and thickness of boundary layers vary across the geometry. The values calculated here are average in space, and for the instant corresponding to each geometry.

MASS TRANSFER GEOMETRY

The metal transfer configuration has several different configurations [29] [30]. In this work we will consider two representative geometries, illustrated in Figure 1. Future work should be able to capture features such as the molten tail in streaming spray transfer.

In solid wire processes, the droplet diameter is often estimated from droplet detachment frequency, neglecting the mass lost to evaporation:

$$d_{\mathrm{MC}} = \left(\frac{3}{2}\frac{\rho c}{\rho}\frac{U_{\mathrm{C}} d_C^2}{f_{MC}}\right)^{1/3} \tag{59}$$

where d_{MC} is the droplet diameter, ρ_{C} is the density of the solid wire, ρ is the density of the melt, U_{C} is the wire feed speed, d_{C} is the wire diameter, and f_{MC} is the frequency of droplet detachment, estimated for the experiments performed using the following empirical expression:

$$f_{\mathrm{MC}} = \begin{cases} CI & \text{for } I \leq I_c \\ AI - B & \text{for } I > I_c \end{cases} \tag{60}$$

where I_{c}, A and B are constants determined empirically, and $C = A - B/I_c$. For ER80S-G, A=1.565 $\mathrm{s^{-1}A^{-1}}$, B=231.8 $\mathrm{s^{-1}}$, and I_{c} =180 A. For aluminum wires A=2.688 $\mathrm{s^{-1}A^{-1}}$, B=319.9 $\mathrm{s^{-1}}$, and I_{c}=128 A. The droplet diameters estimated for the experiments performed are between 0.95 and 2 times the wire diameter.

The area of attachment of the arc to the droplet, in the case of globular and projected spray transfer is approximated as

$$A_{\mathrm{AC,C}} = \pi L_{\mathrm{AC,C}}^2 \tag{61}$$

In the geometry considered, d_{MC} is the droplet diameter and $L_{\mathrm{AC,C}}$ is the attachment of the arc to the electrode. The size of this attachment is a property of the arc, and there are currently no guidelines on how to predict it. In this work, the size of the arc attachment will be estimated based on the knowledge that the arc attachment at the point of transition from globular to spray transfer is comparable to the wire size. Considering the relationship between wire size and transition current proposed in [31] results in the following approximate estimate for the arc attachment:

$$L_{\mathrm{AC,C}} = CI^2 \tag{62}$$

where C=8 10^{-8} m $\mathrm{A^{-2}}$.

TOTAL MASS EVAPORATED

The total mass evaporated at the electrode tip is composed of the sum of all components of the alloy:

$$\dot{m}_v = \sum_j \dot{m}_{v_j} \tag{63}$$

where $\dot{m}_{v_j}$ is the mass rate of evaporation of each alloying element. The stoichiometry of the metal vapors is different than that of the evaporating melt because of the different vapor pressures of each component. For the examples considered here, steel wires containing 1.7 wt% Mn emit vapors with almost 30 wt% Mn, while aluminum wires with 5% Mg emit vapors with almost 75 wt% Mg.

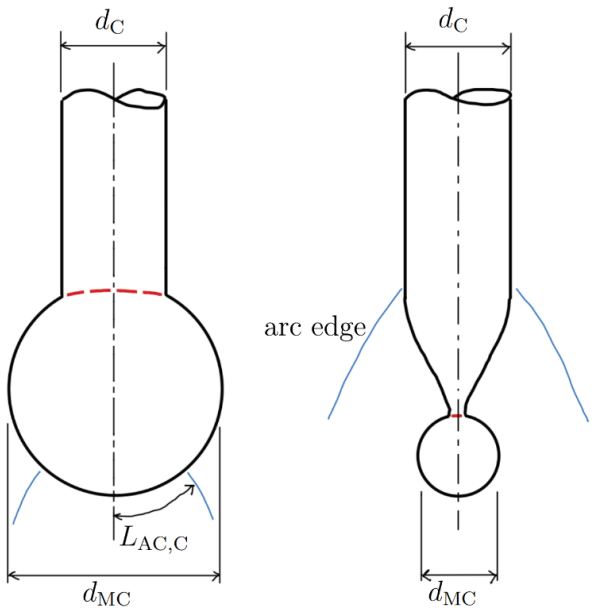

Fig. 1 Representative configurations for globular transfer (left) and spray transfer (right)

The total mass transport must account for the series resistance to mass transfer in the melt, the interphase, and the gas phase as illustrated in Figure 2. It is convenient to start this analysis with the thermal resistance per unit area defined in Equation 5. These considerations result in the following flux:

$$J_j = \frac{p_j}{RT_s\Re''_{\mathrm{tot}_j}} \tag{64}$$

and the corresponding mass flux:

$$\dot{m}''_j = M_j \frac{p_j}{RT_s\Re''_{\mathrm{tot}_j}} \tag{65}$$

where p_j is the vapor pressure in the melt or partial pressure of vapor in the gas phase and $\Re''_{tot_j}$ total mass transfer resistance.

For the solute, the total resistance is made of the equivalent diffusion resistance in the melt, the mass transfer resistance of evaporation, and the diffusion resistance in the gas phase. Because mass transport happens through both liquid and gas phases, the equivalent diffusion resistance defined in Equation 27 must be used for the melt.

$$\Re''_{\mathrm{tot}_{\mathrm{solute}}} = \Re''_{\mathrm{l,eq}_{\mathrm{solute}}} + \Re''_{\mathrm{e\,solute}} + \Re''_{\mathrm{g\,solute}} \tag{66}$$

For the solvent (eg. Fe or Al), there is no resistance to diffusion in the liquid, instead, as the solute (Mn or Mg) depletes, the solvent concentration increases. The flow of solvent involves only resistances of evaporation and in the gas

$$\Re''_{\mathrm{tot}_{\mathrm{solvent}}} = \Re''_{\mathrm{e}\,\mathrm{solvent}} + \Re''_{\mathrm{g}\,\mathrm{solvent}} \tag{67}$$

and the molar and mass flow is calculated using equations 64 and 65 using the vapor pressure of the melt with higher solvent concentration (depleted of solute at the surface).

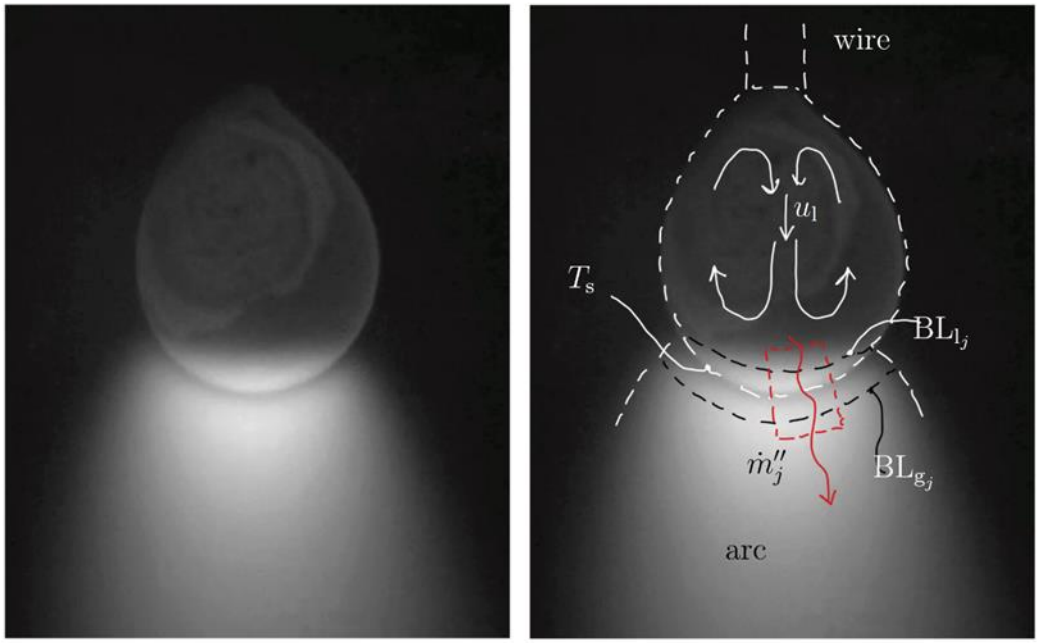

Fig. 2 Tip of molten electrode illustrating the boundary layer in the melt for component *j* (BL_{l_j}), the boundary layer in the gas for component *j* (BL_{g_j}), and the control volume for analysis of mass transfer

RESISTANCE TO MASS TRANSFER IN THE MOLTEN ELECTRODE

The equivalent diffusion resistance per unit area (averaged over the area of diffusion) in the liquid at the electrode tip is calculated based on Equation 27, while the actual resistance is calculated using Equation 18

$$\overline{\Re''_l}_j = \frac{1}{\overline{\mathfrak{h}_{l_j}}} \tag{68}$$

where the diffusion convection coefficient is calculated from the definition of Sherwood number (Equation 42):

$$\overline{\mathfrak{h}_{l_j}} = \frac{\overline{\mathrm{Sh}_{l_j}} D_{l_j}}{d_{\mathrm{MC}}} \tag{69}$$

with $\overline{\mathrm{Sh}_{l_j}}$ being the average Sherwood number for component j in the molten electrode tip, D_{l_j} the diffusivity of component j in the main metal of the molten electrode, and d_{MC} is the diameter of the droplet at the tip of the molten consumable, illustrated in Figure 1. Tabulated parameters to calculate diffusivity in the melt are included in Appendix B.

The average Sherwood number involves a diffusion boundary layer just inside the free surface, such that there is no shear, and the treatment of thermal resistance is according to Section 3.3.2. The expression proposed for $\overline{Sh_{l_j}}$ is the following:

$$\overline{\mathrm{Sh}_{l_j}} = 2 + 0.5\mathrm{Re}_l^{1/2}\mathrm{Sc}_{l_j}^{1/2} \tag{70}$$

where Re_l uses d_{MC} as the characteristic length. This expression is new and was developed for this work, its explanation and its differences with Equation 57 are detailed in this section.

The tip of the molten consumable has a diameter d_{MC} and two boundary layers: one under the free surface (the object of this analysis), and another boundary layer at the solid/liquid interphase, where the electrode is melting. The thickness of both boundary layers is comparable, and they increase in thickness when the fluid motion inside the electrode tip is slow, as $\mathrm{Re}_l \to 0$. When the thickness of these boundary layers reaches half a diameter of the molten consumable, there is no advection region anymore in the melt, and mass transfer occurs just by diffusion. In that case, the Sherwood number of the boundary layer cannot decrease any more, and can be approximated using Equation 42 where the characteristic length is the diameter of the molten tip (d_{MC}), and the thickness of the diffusion layer is half that diameter. Thus, for very small values of Re_l the Sherwood number tends to 2.

At higher Reynolds numbers, the boundary layers are thinner and the Sherwood number increases following the behavior of Equation 57 (top, because there is no shear). The characteristic length in this case is a quarter of the perimeter of the molten tip; each boundary layer affects half the tip (near the free surface, and near the solid/liquid interphase, top and bottom of the molten consumable in Figure 1). Also, because of symmetry, each boundary layer is composed of two parts (left and right). Keeping in mind that average values of Sherwood are twice the local value, the coefficient of 0.5 is obtained.

Given the approximate nature of the analysis and of convection expressions in general, it is not worth to apply blending techniques such as those in [28] to better capture intermediate values of Reynolds numbers. The Reynolds number in this case is

$$\mathrm{Re}_l = \frac{u_l d_{MC}}{v_l} \tag{71}$$

where v_l is the kinematic viscosity of the molten metal at the electrode tip, and u_l is the velocity of the free surface. The velocity of the free surface results from the interplay of

multiple physics including electromagnetic and Marangoni forces. Reference [32] proposes that electromagnetic forces are dominant. In spray transfer, the flow of current envelops the molten tip, such that any induced velocity is small and diffusion dominates over advection. In globular transfer and projected spray, an analysis of electromagnetic forces in the melt is similar to that in the arc performed in [16] resulting in the following approximate expression

$$u_l \approx \frac{1}{\sqrt{\pi}}\sqrt{\frac{\mu_0}{\rho_l}}\left(\frac{1}{d_C}-\frac{1}{2L_{\mathrm{AC,C}}}\right)I \tag{72}$$

where I is the welding current, d_{C} is the diameter of the electrode, $L_{\mathrm{AC,C}}$ is the size of the attachment of the arc indicated in Figure 1, μ_0 is the magnetic permeability of vacuum, and ρ_{l} is the density of the molten metal. This equation accounts for the fact that if the arc attachment is smaller than the electrode diameter the flow moves upwards, and when the arc attachment is of a size comparable to the electrode diameter the electromagnetic forces are small.

For the case of 1.2 mm steel wires, an arc attachment of 2 mm in diameter, and a molten metal temperature of approximately 2000°C ($\rho_l \approx 6500\,\mathrm{kg\,m^{-3}}$), we obtain $u\,(\mathrm{m s^{-1}})$ =1.5x10^{-3} I (A), which is comparable with the value of 2 x10^{-3} proposed in [32].

A survey of GMAW experiments presented in [17] indicates that the range of Sh_l spans from orders of 10^1 to 10^3 in steels and aluminum alloys, indicating that convection dominates over diffusion in the liquid in most cases.

Resistance to mass transfer at the evaporating surface

The resistance to mass transfer at the evaporating surface can be calculated in a straightforward manner using Equation 20.

$$\mathfrak{R}''_{e\,j} = \sqrt{\frac{2\pi M_j}{RT_s}} \tag{73}$$

Resistance to mass transfer in the gas surrounding the molten electrode

For the case of diffusion of metal vapors in an inert atmosphere, such as the evaporation of Fe and Mn in Ar, the thermal resistance (averaged over the area of diffusion) in the gas surrounding the electrode tip is calculated based on Equation 18

$$\overline{\mathfrak{R}''_{\mathrm{g}\,j}} = \frac{1}{\overline{\overline{\mathfrak{h}_{\mathrm{g}_j}}}} \tag{74}$$

where the diffusion convection coefficient is calculated from the definition of Sherwood number (Equation 42):

$$\overline{\mathfrak{h}_{g_j}} = \frac{\overline{\mathrm{Sh}_{g_j}} D_{g_j}}{d_{\mathrm{MC}}} \tag{75}$$

with $\overline{\mathrm{Sh}_{g_j}}$ being the average Sherwood number for component j in the gas surrounding the electrode tip and d_{MC} is the diameter of the droplet at the tip of the molten consumable (Figure 1). The diffusivity D_{g_j} corresponds to component j in the gas surrounding the electrode tip evaluated at a "film temperature" intermediate between the molten surface (of the order of 3000 K for the case of steel and aluminum) and the temperature of the plasma outside the boundary layer near the surface of the electrode (of the order of 7300 K for the case of Ar, resulting in a "film temperature" of approximately 5000 K). Tabulated parameters for the Chapman-Enskog theory to calculate diffusivity in the gas are included in Appendix C.

The average Sherwood number involves a diffusion boundary layer just outside the free surface, such that there is shear of the fast moving gas against the much slower free surface (considered static for this boundary layer). Approximating the electrode tip as a sphere, the Sherwood number of the gas at the tip can be estimated with Equation 58, also used in [33].

$$\overline{\mathrm{Sh}_{g_j}} = 2 + 0.6\mathrm{Re}_{\mathrm{g}}^{1/2}\mathrm{Sc}_{g_j}^{1/3} \tag{76}$$

The Reynolds number in this case is

$$\mathrm{Re}_{\mathrm{g}} = \frac{u_{\mathrm{g}} d_{MC}}{\nu_{\mathrm{g}}} \tag{77}$$

where u_{g} is the velocity of the gas surrounding the free surface, ν_{g} is the kinematic viscosity of the gas surrounding the electrode tip evaluated at a film temperature. The kinematic viscosity and other thermophysical properties for the plasma are provided, for example in [34]. Typical values of $\overline{\mathrm{Sh}_{g_j}}$ are around 10^1, indicating convection is dominant. Typical values of $\mathrm{Re}_{\mathrm{AC}}$ are of the order of 10^2. Schmidt numbers in the vapor are around 1.5.

The velocity u_{g} of gas over the free surface results from the electromagnetic forces present in the arc. In the absence of general correlations, this work will assume that the surface velocity of the gas is the maximum velocity in the arc. This maximum velocity was studied in [16] for the GTAW arc, and will be extended to the GMAW arc, acknowledging the uncertainties in this extrapolation.

$$u_{\mathrm{g}} = \frac{1}{2\pi}\sqrt{\frac{\mu_0}{\rho_{\mathrm{AC}}}}\frac{I}{L_{AC,C}} f_{\mathrm{u_g}} \tag{78}$$

where ρ_{AC} is the density of the gas in the arc column (at approximately 10^4 K), and f_{u_g} is a correction factor defined as

$$f_{\mathrm{u_g}} = 0.55\left(\frac{\widehat{\mathrm{Re}}_{\mathrm{AC}}}{4}\right)^{0.073}\left(\frac{2L_{\mathrm{arc}}}{d_C}\right)^{0.0068} \tag{79}$$

with $\widehat{\mathrm{Re}}_{\mathrm{AC}}$ being a nominal Reynolds number calculated using the velocity Eq. 78 without the correction factor $f_{\mathrm{u_g}}$ and the diameter of the molten tip d_{MC} as a characteristic length. The magnitude ν_{AC} is the kinematic viscosity of the plasma at the plasma column temperature (approximately 10^4 K). The arc length in the experiments made was set at 0.5 in. (12.7 mm), this is a value much longer than typically used in practice but needed to get temperature measurements with the setup used.

EVAPORATION FLOWS FROM THE ELECTRODE TIP

For the overall flux of component *j*, Equation 7 becomes

$$\bar{J}_j = \frac{p_{\mathrm{l}_j}}{RT_{\mathrm{s}}\overline{\Re''_{\mathrm{tot}_j}}} \tag{80}$$

where p_{l_j} is the vapor pressure at the nominal composition in the bulk of the molten electrode tip, and the vapor pressure of j outside the diffusion boundary layer is 0. In steels and aluminum alloys, the dominant resistance to evaporation of the main component (Fe or Al) is the gas boundary layer (above approximately 95% of total resistance), while for the solute evaporation (Mn or Mg) the resistance of evaporation at the surface is negligible, and the resistance in the melt and in the gas are comparable (typically the resistance in the melt is higher). This is an important finding indicating the importance of boundary layers in mass loses by evaporation, which have been omitted in the welding literature.

CONCENTRATION PROFILES

Concentrations in the melt and in the gas can be obtained using a standard calculation with mass transfer resistances.

For solute at the surface of the melt:

$$c_{\mathrm{l},s_{\mathrm{solute}}} = c_{\mathrm{l}_{\mathrm{solute}}} - J_{\mathrm{solute}}\Re''_{\mathrm{l}\ \mathrm{solute}} \tag{81}$$

where J_{solute} is calculated using Equation 26 and equivalent vapor pressures for the melt.

For the solvent, at the free surface of the melt the fraction of solvent is higher because of depletion of solute. Converting the concentration of solute at the surface $c_{l,s_{\mathrm{solute}}}$ to molar fraction ($X_{l,s_{\mathrm{solute}}}$), the molar fraction of solvent is

$$X_{l,s_{\mathrm{solvent}}} = 1 - \sum_j X_{l,s_{\mathrm{solute},j}} \tag{82}$$

In the gas phase it is more convenient to discuss concentration profiles in terms of partial pressure of vapors. The partial pressure of vapors against the free surface can also be

calculated for both solute and solvent using Equation 7, accounting for a zero concentration of metal vapor outside the boundary layer:

$$p_{\mathrm{g,s}_j} = RT_s J_j \mathfrak{R}''_{\mathrm{g}\,j} \tag{83}$$

The overall mass flow of component j is given by Equation 11 using the area of arc attachment $A_{\mathrm{AC,C}}$ (Equation 61), which is an approximation useful for the metal transfer conditions of the experiments performed.

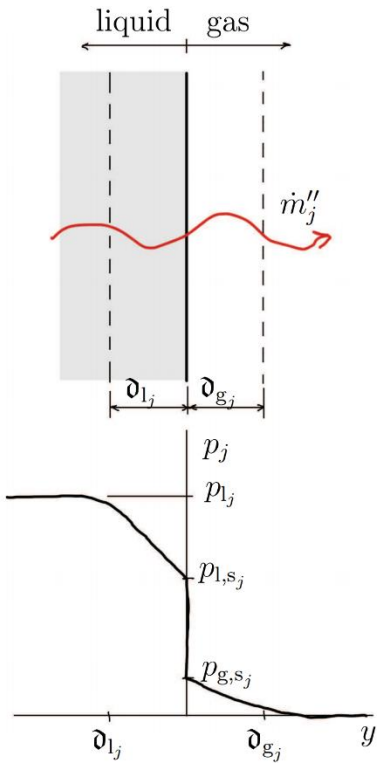

Fig. 3 Concentration profile for solute component j. Gradient in the liquid is due $\mathfrak{R}''_{\mathrm{l}\,j}$, gradient in the gas is due to $\mathfrak{R}''_{\mathrm{g}\,j}$, and the discontinuity at the free surface is due to $\mathfrak{R}''_{\mathrm{e}\,j}$

EXAMPLE OF APPLICATION

A set of experiments was performed, reported in [17, 35]. Three experiments are selected: E1 for steel consumable ER80S-G (1.7 wt% Mn), E2 for aluminum alloy 5554 (2.7 wt% Mg), and E3 for aluminum 5183 (4.9 wt% Mg). The temperature of the droplet was measured.

EXPERIMENTS AND PROCESS CONDITIONS

Process conditions and measured temperatures are listed in Table 1, properties of the molten electrode tip are listed in Table 2, and properties of the gas and vapors are listed in Table 3. The properties used for diffusion in the melt indicate that diffusivity of Mg in molten Al is about two orders of magnitude faster than the diffusivity of Mn in molten Fe. This result is surprising, but comparisons with other source for diffusivity in the iron [36] yield similar results. This large difference in diffusivity values also results in large differences in Sc and Sh numbers between steel and aluminum.

Table 1 Process parameters

Exp.	Consumable	f_{solute} * wt%	X_{solute} * mol%	d_C mm	U_C cm min^{-1}	U_C m s^{-1}	I A
E1	ER80S-G	1.74	1.77	1.20	454	7.56 10^{-2}	161
E2	5554	2.66	2.94	1.18	642	1.07 10^{-1}	141
E3	5183	4.93	5.44	1.19	612	1.02 10^{-1}	130

*solute is Mn and solvent Fe for ER80S-G, solute is Mg and solvent Al for 5554 and 5183

Table 2 Properties of molten electrode tip

Exp.	T_s ℃	M* g mol^{-1}	ρ_C † kg m^{-3}	ρ kg m^{-3}	ν m^{2}s^{-1}	$D_{l_{solute}}$ m^{2}s^{-1}	$Sc_{l_{solute}}$
E1	2313	55.8	7830	5424	3.03 10^{-7}	5.37 10^{-9}	56
E2	2210	26.9	2703	1838	2.64 10^{-7}	2.01 10^{-6}	0.13
E3	1730	26.8	2703	2006	2.81 10^{-7}	6.82 10^{-7}	0.41

*molar mass of components in Table3
† solid wire at 20 ℃

The process conditions at the molten electrode tip are listed in Table 4. The molten metal temperature typically exceeds by far the meting temperature, especially for aluminum. The estimated liquid metal velocities are of the order of 0.5 m s^{-1} and the Reynolds number of the order of 10^3, consistent with the 0.2 m s^{-1} and 500 estimated in [32].

The process conditions in the arc are listed in Table 5. The plasma velocity is surprisingly smaller than the 300 m s^{-1} typical of GTAW. Equation 78 suggests that this is due to the lower plasma temperature (higher gas density) and the larger attachment of the arc to the electrode.

Table 3 Properties of shielding gas and vapors

Exp.	Solute §	M_{solute} g mol^{-1}	$D_{g_{\text{solute}}}$ * m^2s^{-1}	$Sc_{g_{\text{solute}}}$ *
E1	Mn	54.94	1.96 10^{-3}	0.861
	Fe	55.85	1.98 10^{-3}	0.853
E2, E3	Mg	24.31	2.10 10^{-3}	0.803
	Al	26.98	2.22 10^{-3}	0.761

§ solvent always is Ar
M_{Ar} =39.95 kg mol^{-1}
v_{g} =1.69 10^{-3} m^2s^{-1}∗
v_{AC} = 5.53 10^{-3} m^2s^{-1} †
ρ_{AC} = 47.7 10^{-3} m^2s^{-3} †
* at T_{film} = 5000 K [37]
† at T_{AC} = 10000 K [37]

Table 4 Process conditions at the molten electrode tip

Exp.	T_s†		d_{MC}	f_{MC}	$L_{\text{AC,C}}$	$A_{\text{AC,C}}$	u_1	Re_1
	℃	K	mm	Hz	mm	m^2	m s^{-1}	
E1	2313	2586	1.64	44.7	2.10	1.36 10^{-5}	0.463	2.66 10^3
E2	2210	2483	1.73	58.0	1.58	7.86 10^{-6}	0.622	4.21 10^3
E3	1730	2003	2.17	28.7	1.35	5.69 10^{-6}	0.484	3.73 10^3

† from [17]

Table 5 Process conditions in the arc

Exp.	u_g m s^{-1}	f_{u_g}	Re_g	$\widehat{Re}_{AC}$
E1	40.0	0.631	41.2	20.0
E2	46.4	0.639	48.9	23.4
E3	51.3	0.652	65.8	30.8

arc length set to L_{arc} =12.7 mm

MASS TRANSFER MAGNITUDES

The mass transfer resistances obtained are listed in Table 6. The N/A values for resistance for Fe or Al in the melt is because they are the solvent. In all cases the resistance of evaporation

is negligible. The resistance for mass transfer of solute in the melt is always larger than that in the gas phase, but the resistance in the gas phase cannot be neglected.

Table 7 contains the mass transfer magnitudes associated with each experiment and component. The Sherwood numbers for diffusion in the melt and the gas are large, confirming the relevance of advection over bulk diffusion. The large difference in the values of $\mathfrak{h}_{l_j}$ and $\mathfrak{h}_{g_j}$ is because they are based on different reference systems, one in the liquid phase and another in the gas phase. The thickness of the boundary layers in the melt are different by an order of magnitude between steel and aluminum consumables. This large difference might be due to the very different diffusivities in molten Fe and Al. The boundary layer thickness in the gas phase is consistent around 300 μm.

Table 6 Mass transfer resistances

Exp.	Comp.	$\mathfrak{R}''_l$ s m^{-1}	$\mathfrak{R}''_{l,eq}$ s m^{-1}	$\mathfrak{R}''_e$ s m^{-1}	$\mathfrak{R}''_g$ s m^{-1}	$\mathfrak{R}''_{tot}$ s m^{-1}	$\mathfrak{R}''_{l,eq}$ %	$\mathfrak{R}''_e$ %	$\mathfrak{R}''_g$ %
E1	Mn	1.66 10^3	0.241	4.01 10^{-3}	0.157	0.401	60	1.00	39
	Fe	N/A	N/A	4.01 10^{-3}	0.155	0.159	N/A	2.53	97
E2	Mg	6.45 10^1	0.731	2.72 10^{-3}	0.144	0.877	83	0.31	16
	Al	N/A	N/A	2.87 10^{-3}	0.138	0.140	N/A	2.04	98
E3	Mg	1.47 10^2	0.427	3.03 10^{-3}	0.158	0.588	73	0.52	27
	Al	N/A	N/A	3.19 10^{-3}	0.155	0.155	N/A	2.06	98

Table 7 Mass transfer magnitudes

Exp.	Comp.	Sh_{l_j}	Sh_{g_j}	$\mathfrak{h}_{l_j}$ m s^{-1}	$\mathfrak{h}_{g_v}$ m s^{-1}	$\mathfrak{d}_{l_j}$ μm	$\mathfrak{d}_{g_j}$ μm
E1	Mn	196	5.66	6.03 10^{-4}	6.39	8.90	307
	Fe	196	5.65	6.03 10^{-4}	6.43	8.90	308
E2	Mg	13.7	5.90	1.55 10^{-2}	6.97	130	302
	Al	13.7	5.83	1.55 10^{-2}	7.27	130	306
E3	Mg	21.6	6.52	6.80 10^{-3}	6.34	100	332
	Al	21.6	6.44	6.80 10^{-3}	6.61	100	336

Table 8 contains the flux, compositions, and partial pressures associated with mass transfer in the experiments. The results show a significant depletion of solute on the surface of the droplet, e.g. only 0.7 wt% Mn in ER80S-G, when it was originally 1.74 wt%; conversely, the solvent is slightly enriched.

The value of p_{lg_j} corresponds to the vapor pressure of the pure component at the temperature of the melt (listed in Table 4); this pressure is theoretical, and not experienced anywhere in the welding process.

The pressure p_{l,s_j} corresponds to the vapor pressure of the component as part of the alloy at the molten tip of the electrode. This pressure is real, but it will manifest only if gas is nucleated in the molten metal. It can be seen that p_{l,s_j} is quite small for the solvent component (Fe, Al);

this makes sense considering that droplet temperature in GMAW is typically below boiling temperature [17, 35, 38, 39, 40, 41, 42, 43].

For Mn in steel, the vapor pressure in solution is also low; however, for Mn in aluminum alloys, the vapor pressure exceeds one atmosphere. If a Mg vapor bubble nucleates, its high pressure will make it burst causing explosive transfer, as studied in [8]. Figure 4 shows stages of explosive transfer from the experiments in this work. The experiments showed the absence of explosive transfer in the steel wire (E1), the highest intensity of explosive transfer in E2 (Al alloy with lower amount of Mg, but higher temperature), and moderate amount of explosive transfer in E3.

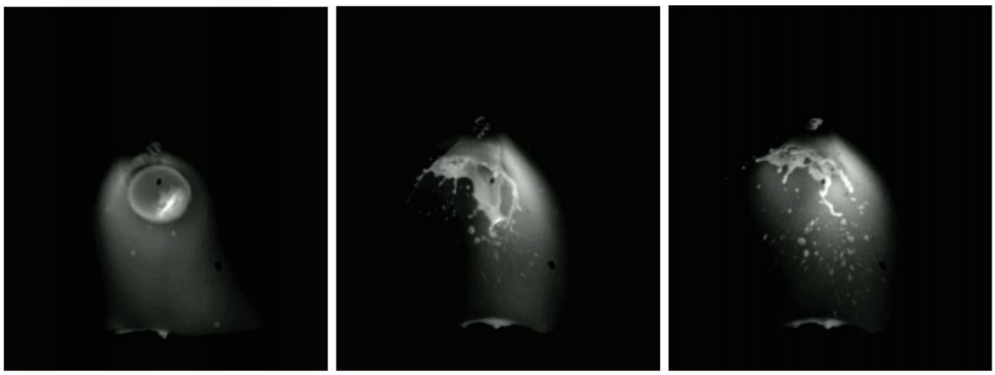

Fig. 4 Three stages of explosive transfer in 5554 Aluminum alloy

At the free surface, p_{l,s_j} and p_{g,s_j} represent the vapor pressure on the melt and the gas side. In all cases, the vapor pressure in the surface of the melt is below boiling, this is because the resistance to diffusion in the melt depletes the solute (Mn or Mg) from the surface, and with lower solute content, the lower the vapor pressure. The vapor pressure for the solvent is slightly increased as the fraction of solvent is higher at the free surface. at the free surface, the pressure difference between liquid and solid is small, consistently with the small value associated with resistance of evaporation.

Table 8 Compositions and partial pressures

Exp.	Comp.	J_j	X_{l,s_j}	f_{l,s_j}	p_{lg_j}	p_{l_j}	p_{l,s_j}	p_{g,s_j}
		mol $s^{-1}m^{-2}$	mol%	wt%	atm	atm	atm	atm
E1	Mn	0.62	0.71	0.70	3.00	$5.3\ 10^{-2}$	$2.12\ 10^{-2}$	$2.07\ 10^{-2}$
	Fe	1.76	99.3	99.3	$5.99\ 10^{-2}$	$5.89\ 10^{-2}$	$5.95\ 10^{-2}$	$5.80\ 10^{-2}$
E2	Mg	26.0	0.49	0.44	158	4.64	$7.74\ 10^{-1}$	$7.59\ 10^{-1}$
	Al	8.38	99.5	99.6	$2.41\ 10^{-1}$	$2.35\ 10^{-1}$	$2.40\ 10^{-1}$	$2.35\ 10^{-1}$
E3	Mg	20.1	1.49	1.35	35.7	1.94	$5.31\ 10^{-1}$	$5.21\ 10^{-1}$
	Al	0.25	98.5	98.7	$6.57\ 10^{-3}$	$6.25\ 10^{-3}$	$6.47\ 10^{-3}$	$6.34\ 10^{-3}$

Table 9 contains the estimated mass flux of Fe, Mn, Al, and Mg in the experiments performed. The amount of Mn lost in the steel alloy is almost 4 wt% of the initial value, resulting in a final composition of 1.67 wt% of Mn, down from the original 1.74 wt% listed in Table 1. The fraction loss of Fe is much lower, but because it is the bulk of the alloy, the small amount of evaporation is significant. The total mass loss to evaporation estimated in the steel experiment is 0.27 wt%. The destination of these metal vapors is in the form of the dust that covers weld shops, but more importantly, in the form of toxic fume that could be breathed if there is insufficient protection in the workspace. Because of the higher evaporation rate, the metallic composition of the fumes is expected to be 26 wt% Mn, much higher than the original alloy stoichiometry. This high value is consistent with reports in the analysis of welding fumes, such as [2]. The exact value is difficult to measure accurately and is the subject of current work.

The amount of Mg lost in the aluminum alloys much higher than in steel, almost 60% loss for E2, which experienced the highest temperature, and almost 20% loss for E3. The material deposited in E2 is estimated to have only 1.1 wt% Mg, instead of the nominal 2.66 wt%. Similarly, for experiment E3 the deposit is estimated as 4.06 wt% Mg instead of 5.44 wt%. These low values of recovery should be confirmed with carefully done experiments. The total mass loss to evaporation estimated in the aluminum experiments is much higher than in steel, approximately 2 wt% for the very hot experiment E2 and almost 1 wt% for the high alloy of Experiment E3. The metallic composition of the fumes is expected to be 74 wt% Mg in E2 and 98 wt% in E3. This very high last value needs to be confirmed. In Al-Mg alloys, in addition to the toxic fumes, the metal vapors condense as undesirable black oxides called “smut” in the weld shops. Cleaning smut is a costly operation.

The recoil pressure associated with the mass loss is mostly associated with the solvent (Fe) in the steel wire, and with the solute (Mg) in the Al-Mg wires. The recoil pressures, of the order of 10^{-3} atm to 10^{-2} atm seem small; however, they are enough to levitate the droplet.

Table 9 Mass balances and recoil pressure

Exp.	Comp.	$\dot{m}_j''$	$\dot{m}_j$	f_{evap_j}	$f_{\text{evap}_{\text{tot}}}$	f_{deposit}	f_{fumes} *	p_{rec}	$p_{\text{rec,total}}$
		kg s^{-1}m^{-2}	kg s^{-1}	wt%	wt%	wt%	wt%	Pa	Pa
	Mn	3.42 10^{-2}	4.63 10^{-7}	3.98			26.0	21.4	
E1					0.27	1.67			82.3
	Fe	9.72 10^{-2}	1.32 10^{-6}	0.20			74.0	60.9	
	Mg	6.31 10^{-1}	4.96 10^{-6}	58.9			74.0	582	
E2					2.12	1.10			779
	Al	2.21 10^{-1}	1.74 10^{-6}	0.56			26.0	198	
	Mg	4.89 10^{-1}	2.78 10^{-6}	18.4			98.7	404	
E3					0.92	4.06			410
	Al	6.64 10^{-3}	3.78 10^{-8}	0.01			1.34	5.40	

*balance of metals only, excluding oxygen

DISCUSSION

The analysis presented is the first comprehensive treatment of diffusion in the welding process accounting for transport in bo the the melt and the shielding gases. A number of simplifications were needed to arrive to the conclusions, and future work will provide a better treatment of particular aspects. None of the conclusions is expected to change, but quantitative analysis can be made more reliable and general. Some areas for future improvement are the following:

- Better treatment of heat transfer in the melt and arc, especially considering diffusion in thermal gradients. In this work, the molten consumable is treated as isothermal, as well as the gases surrounding the melt, where diffusion on the gas is present. Temperature gradients on the melt surface would be of much influence on what is considered the active area of evaporation.
- Confirm or improve the values of diffusivity in melt. The values obtained for diffusivity in molten steel are approximately two orders of magnitude lower than those in molten aluminum. While this large difference is possible, it should be verified with additional sources and theoretical analysis.
- Generalize treatment to multi-principal component alloys. In this work, an alloying component is dominant, such as Fe or Al, while the other components are small fractions of the total. Commercial alloys such as Inconel 718 and many others lack a single component that can be considered a ``solvent,'' so a more general definition of solvent should be used.

- Account for advection in gas diffusion, especially as the vapor pressure approaches the atmospheric pressure. This work considers only advection associated with the boundary layer (parallel to the surface); however, during evaporation there is another source of advection perpendicular to the surface that eventually becomes dominant at temperatures approaching boiling. There is a conventional treatment that does not account for the high recoil pressure often found in welding. This improved treatment requires special expertise in mass transfer in gases, and perhaps an expansion on what is already known.
- Validate evaporation data against existing and new experiments. The treatment presented here makes predictions of amount of metal vapors and compositions. These magnitude are measurable, but not simply. The amount of fumes is measured with standards such as AWS F1.2 “Laboratory Method for Measuring Fume Generation Rates and Total Fume Emission of Welding and Allied Processes”, which is suitable for relative magnitudes, but not accurate for mass balances. Similarly, measuring the metal balance in fumes involves complexities such as separating spatter particles and other contamination. Both challenges are surmountable, but require a dedicated experimental effort and expertise.
- Improve the treatment of droplet temperature and geometry of metal transfer including streaming spray. There is currently no theory that can predict droplet temperature reliably or the geometry of metal transfer. For the case of GMAW, there is no theory predicting the length of the tail in streaming spray transfer, which is likely to affect the temperature of the molten consumable.
- Extend analysis to weld pool and other geometries. For the weld pool in particular, jet impingement heat transfer correlations exist, which could be extended to mass transfer calculations. There are previous studies of evaporation on the weld pool surface such as [6] that should be compared directly.

CRITERION FOR EXPLOSIVE TRANSFER

Based on the analysis and observations, a general criterion for explosive transfer can be proposed: Explosive transfer is possible when the vapor pressure of components in the melt reaches the atmospheric pressure. Because the explosion in the droplet requires nucleation of a vapor bubble, it is possible that alloys with impurities that can act as nucleants are more prone to explosive transfer.

Mitigation of explosive transfer can be attempted with lower droplet temperatures, lower alloying content, and higher boiling temperature of the components. Lower droplet temperatures is the most important factor, and can be reached with pulsing. Lower alloying component and higher boiling temperatures might not be possible within alloy specifications. Another possible mitigation strategy is reducing the time in which an element of molten consumable is exposed to high temperatures, for example in streaming transfer in which the melt flows rapidly through a cone, a potential tail, to detach quickly small droplets.

MITIGATION OF FUME FORMATION

The model presented indicates that a lower droplet temperature is the most important factor also for fume generation. In CV GMAW, the droplet temperature reaches a minimum around the globular to spray transition [17, 35, 38, 39, 42] which is consistent with a minimum in measure fume formation rates [3, 4].

Because droplet temperature increases during the metal transfer process, pulsing can cause droplet detachment before the droplet gets too hot and starts emitting a high rate of fumes.

A lower droplet temperature also implies a lower proportion of volatile elements in the fumes, e.g. lower amount of Mn in fumes of steel welding. Of course, smaller droplets also present lower area of evaporation; however, in streaming spray, the molten tail (not treated in this work) also generates fumes, resulting in a high volume of fumes even when the droplets are small.

In all cases, the boundary layer in the gas plays an important role in the rate of fume generation. Although there is no direct way of controlling this boundary layer without affecting the overall process, a thinner gas boundary layer is likely to result in higher fumes. One of the ways in which the gas boundary layer is undesirably thinned is in the presence of chemical reactions such as oxidation (not treated in this work). It is known that the presence of oxygen in the shielding gases in GMAW results in higher fume formation rate.

CONCLUSIONS

This paper presents for the first time a comprehensive treatment of mass transfer and evaporation in welding; in particular, the simultaneous barriers to mass transfer in the molten metal, at the evaporating surface, and in the surrounding gases are considered.

Multicomponent mass transfer is considered, and explicit expressions for the resistance to mass transfer for each component and each stage are provided. A novel treatment for diffusion in the melt is proposed by using an equivalent mass transfer resistance in the melt; this treatment is based on the vapor pressure of each component in the melt, and allows for the simultaneous consideration of all mass transfer resistances. The treatment of mass transfer also includes a treatment of recoil pressure.

The particular case of mass transfer and evaporation in the electrode tip in GMAW is considered, and three experiments are analyzed in detail. The results obtained are consistent with observations.

A criterion for explosive transfer is proposed based on the vapor pressure of components in the melt exceeding the pressure surrounding the wire tip (usually atmospheric), reproducing the type and amount of explosions observed.

The treatment of mass transfer presented is enabling for a comprehensive formulation of mass and energy balances and for theoretical treatment of fume generation, which is a topic of large impact in welding practice.

Despite the depth of the treatment, the work presented is more of a foundation than a complete treatment, with concrete suggestions for improvement in the Discussion section.

ACKNOWLEDGEMENTS

This work builds on the effort and talent of many graduate and undergraduate students over decades. Much gratitude to Nitheesh Kumar for compiling and validating the tabulated molten metal and plasma properties in the appendices and to Nitheesh and Xinrui Liu for translating this very complex document from LaTeX into MS Word.

References

[1] H. R. CASTNER: 'Gas Metal Arc Welding Fume Generation Using Pulsed Current', *Welding Journal*, pp. 59s-68s, 1995.

[2] N. T. JENKINS: *Chemistry of Airburne Particles from Metallurgical Processing*, Doctor of Philosophy, MIT, 2003.

[3] P. F. MENDEZ, N. T. JENKINS, and T. W. EAGAR: 'Effect of Electrode Droplet Size on Evaporation and Fume Generation in GMAW', in *Gas Metal Arc Welding for the 21st Century*, Orlando, FL, American Welding Society, pp. 325-332, 2000.

[4] N. T. JENKINS, P. F. MENDEZ, and T. W. EAGAR: 'Effect of Arc Welding Electrode Temperature on Vapor and Fume Composition'," in *Trends in Welding Research*, Pine Mountain, GA, 2005.

[5] A. BLOCK-BOLTEN and T. W. EAGAR: 'Metal Vaporization from Weld Pools', *Metallurgical Transactions B*, vol. 15B. pp. 461-469, 1984.

[6] R. T. C. CHOO, J. SZEKELY, and S. A. DAVID: 'On the Calculation of the Free Surface Temperature of Gas-Tungsten-Arc Weld Pools from First Principles: Part II. Modeling the Weld Pool and Comparison with Experiments', *Metallurgical Transactions B*, vol. 23B, pp. 371-384, 1992.

[7] T. DEBROY, S. BASU, and K. MUNDRA: 'Probing Laser-Induced Metal Vaporization by Gas-Dynamics and Liquid Pool Transport Phenomena', *Journal of Applied Physics*, vol. 70, no. 3, pp. 1313-1319, 1991.

[8] U. REISGEN *et al.*: 'Task of volumetrical evaporation and behaviour of droplets in pulsed MIG welding of Al Mg alloys', *Welding in the World*, vol. 57, pp. 507-514, 2013.

[9] T. BERGMAN, A. LAVINNE, F. INCROPERA, and D. DEWITT: *Introduction to Heat Transfer*, Sixth, New Jersey, United States: John Willey and Sons, 2002.

[10] J. MCKELLIGET and J. SZEKELY: 'Heat Transfer and Fluid Flow in the Welding Arc', *Metallurgical Transactions A*, vol. 17A, pp. 1139-1147, 1986.

[11] G. M. POUND: 'Selected Values of Evaporation and Condensation Coefficients for Simple Substances', *J. Phys. Chem. Ref. Data*, vol. 1, no. 1, 1972.

[12] C. PERROTT: 'The role of electrode vaporization in GMA welding', *Welding Technology*, vol. 82, pp. 299-309, 1982.

[13] J. F. LANCASTER: *The Physics of Welding*, 2nd ed. Pergamon Press, 1986.

[14] C. XI and W. HAI-XING: 'A calculation model for the evaporation recoil pressure in laser material processing', *Journal of Physics D: Applied Physics*, vol. 34, no. 17, p. 2637, 2001.

[15] J. SAFARIAN and T. A. ENGH: 'Vacuum evaporation of pure metals', *Metallurgical and Materials Transactions A*, vol. 44, no. 2, pp. 747-753, 2013.

[16] P. F. MENDEZ, M. A. RAMIREZ, G. TRAPAGA, and T. W. EAGER: 'Order-of-magnitude scaling of the cathode region in an axisymmetric transferred electric arc', *Metallurgical and Materials Transactions B-Process Metallurgy and Materials Processing Science*, vol. 32, no. 3. pp. 547-554, 2001.

[17] P. F. MENDEZ, Z. YAN, V. N. SÁNCHEZ, and S. CHEN: 'Physical Mechanisms Governing Deposition Rate in Arc Welding with a Consumable Electrode', in *Mathematical Modelling of*

Weld Phenomena 13, C. Sommitsch, N. Enzinger, and P. Mayr, Eds., Graz-Seggau, Austria: Verlag der Technischen Universität Graz, 2022.

[18] E. TURKDOGAN, P. GRIEVESON, and L. DARKEN: 'The formation of iron oxide fume', *JOM*, vol. 14, no. 7. pp. 521-526, 1962.

[19] E. TURKDOGAN, P. GRIEVESON, and L. DARKEN: 'Enhancement of diffusion-limited rates of vaporization of metals', *The Journal of Physical Chemistry*, vol. 67, no. 8. pp. 1647–1654, 1963.

[20] S. E. FERREE: 'New generation of cored wires creates less fume and spatter', *Welding Journal*, vol. 74, no. 12. pp. 45-49, 1995.

[21] K. CARPENTER, B. MONAGHAN, and J. NORRISH: 'Influence of Shielding Gas on Fume Formation Rate For Gas Metal Arc Welding of Plain Carbon Steels', *Trends in Welding Research*. pp. 436-442, 2009.

[22] R. T. C. CHOO and J. SZEKELY: 'The Possible Role of Turbulence in GTA Weld Pool Behavior', *Welding Journal*, pp. 25s-31s, 1994.

[23] H. SCHLICHTING: *Boundary-layer theory*, 7th ed. in McGraw-Hill classic textbook reissue series, New York: McGraw-Hill, 1987.

[24] P. F. MENDEZ: 'Calculation of thermal features in welding and additive manufacturing', in *Modelling of Casting, Welding and Advanced Solidification Processes, MCWASP*, Banff, AB, 2023.

[25] A. B. MURPHY: 'A comparison of treatments of diffusion in thermal plasmas', *Journal of Physics D: Applied Physics*, vol. 29, no. 7, p. 1922, 1996.

[26] A. B. MURPHY: 'Treatments of diffusion in thermal plasmas', *High Temperature Material Processes: An International Quarterly of High-Technology Plasma Processes*, vol. 4, no. 1, 2000.

[27] A. B. MURPHY: 'Calculation and application of combined diffusion coefficients in thermal plasmas', *Scientific Reports*, vol. 4, no. 1, p. 4304, 2014.

[28] P. F. MENDEZ: 'Reduced order models for welding and solidification processes', *15th International Conference on Modelling of Casting, Welding and Advanced Solidification Processes, MCWASP*, vol. 861. p. 012003, 2020.

[29] A. SCOTTI, V. PONOMAREV, and W. LUCAS: 'A scientific application oriented classification for metal transfer modes in GMA welding', *Journal of Materials Processing Technology*, vol. 212, no. 6, pp. 1406-1413, 2012.

[30] J. NORRISH: 'A review of metal transfer classification in arc welding (IIW DOC. XII-1769-03. Bucharest)', *Villepinte, France: International Institute of Welding*, 2003.

[31] J. LOWKE: 'Globular and Spray Transfer in MIG Welding', *Welding in the World*, vol. 55, pp. 19-23, 2011.

[32] J. H. WASZINK and G. J. P. M. VAN DEN HEUVEL: 'Heat Generation and Heat Flow in the Filler Metal in GMA Welding', *Welding Journal*. pp. 269s-282s, 1982.

[33] C. REDDING: 'Fume model for gas metal arc welding', *Welding Journal*, vol. 81, no. 6, pp. 95-S, 2002.

[34] A. B. MURPHY and C. ARUNDELL: 'Transport coefficients of argon, nitrogen, oxygen, argon-nitrogen, and argon-oxygen plasmas', *Plasma Chemistry and Plasma Processing*, vol. 14. pp. 451-490, 1994.

[35] Z. YAN, K. SCOTT, S. CHEN, and P. MENDEZ: 'Deposition Rate in GMAW of ER1100 and ER5183 Aluminum Alloys', *Welding Journal*, vol. 101. pp. 289s-292s, 2022.

[36] B. ZHANG: 'Calculation of self-diffusion coefficients in iron', *AIP Advances*, vol. 4, no. 1, 2014.

[37] A. B. MURPHY and E. TAM: 'Thermodynamic properties and transport coefficients of arc lamp plasmas: argon, krypton and xenon', *Journal of Physics D: Applied Physics*, vol. 47, no. 29, p. 295202, 2014.

[38] E. SODERSTROM, K. M. SCOTT, and P. F. MENDEZ: 'Calorimetric Measurement of Droplet Temperature in GMAW', *Welding Journal*, vol. 90, no. 4. pp. 77s-84s, 2011.
[39] K. M. SCOTT: *Heat Transfer and Calorimetry of Tubular Ni/WC Wires Deposited with GMAW*, MSc, University of Alberta, 2011.
[40] J. CHAPUIS, K. M. SCOTT, S. D. GUEST, E. SODERSTROM, and P. F. MENDEZ: 'Temperature and Size Measurements of Droplet During Free Flight Gas Metal Arc Welding (Mesures de température et de taille de goutte en vol libre lors d'une opération de soudage MIG-MAG)', *Canadian Welding Association Annual Conference*. 2011.
[41] J. CHAPUIS, K. M. SCOTT, S. D. GUEST, E. SODERSTROM, and P. F. MENDEZ: 'Droplet Calorimetry and High Speed Videography of Free Flight Metal Transfer in Gas Metal Arc Welding', *IIW Annual Assembly*. p. Doc.212-1232-12, 2012.
[42] C. MCINTOSH, J. CHAPUIS, and P. F. MENDEZ: 'Effect of Ar-CO2 Gas Blends on Droplet Temperature in GMAW', *Welding Journal*, vol. 95, no. 8. pp. 273s-279s, 2016.
[43] C. MCINTOSH and P. F. MENDEZ: 'Fall Voltages in Advanced Waveform Aluminum GMAW', *Welding Journal*, vol. 96. pp. 354s–366s, 2017.
[44] T. SAITO, Y. KAWAI, K. MARUYA, and M. MAKI: 'Diffusion of some alloying elements in liquid iron', *Sci. Rep. Res. Inst. Tohoku Univ. Ser. A Phys. Chem. Metall*, vol. 11, pp. 401-410, 1959.
[45] Y. DU *et al.*: 'Diffusion coefficients of some solutes in fcc and liquid Al: critical evaluation and correlation', *Materials Science and Engineering: A*, vol. 363, no. 1-2, pp. 140-151, 2003.
[46] M. R. BELLÉ *et al.*: 'Density, Surface Tension, and Viscosity of Liquid Low-Sulfur Manganese–Boron Steel via Maximum Bubble Pressure and Oscillating Crucible Methods', *Steel Research International*, vol. 96, no. 5, p. 2400252, 2025.
[47] A. DINSDALE and P. QUESTED: 'The viscosity of aluminium and its alloys–A review of data and models', *Journal of Materials Science*, vol. 39, no. 24, pp. 7221-7228, 2004.
[48] P. M. SMITH, J. W. ELMER, and G. F. GALLEGOS: 'Measurement of the density of liquid aluminum alloys by an X-ray attenuation technique', *Scripta Materialia*, vol. 40, no. 8, pp. 937-941, 1999.
[49] C. R. REID, J. M. PRAUSNITZ and B. E. POLING: 'The Properties of Gases and Liquids', McGraw-Hill, 1987.
[50] D. R. POIRIER and G. GEIGER: *Transport phenomena in materials processing*, Springer, 2016.
[51] R. C. REID, J. M. PRAUSNITZ and B. E. POLING: *The properties of gases and liquids*. McGraw Hill Book Co.,New York, NY, 1986, [Online] Available: https://www.osti.gov/biblio/6504847.
[52] E. TURKDOGAN: 'Diffusivities of gases and metal vapors at elevated temperatures', in *Steelmaking: The Chipman Conference*, MIT Press Cambridge, Mass., 1965, pp. 77-87.
[53] C. B. ALCOCK, V. ITKIN, and M. HORRIGAN: 'Vapour pressure equations for the metallic elements: 298-2500K', *Canadian Metallurgical Quarterly*, vol. 23, no. 3, pp. 309-313, 1984.
[54] T. TOMOOKA, Y. SHOJI, and T. MATSUI: 'High temperature vapor pressure of Si', *Journal of the Mass Spectrometry Society of Japan*, vol. 47, no. 1, pp. 49-53, 1999.
[55] P. D. DESAI: 'Thermodynamic properties of manganese and molybdenum', *Journal of Physical and Chemical Reference Data*, vol. 16, no. 1, pp. 91-108, 1987.

APPENDICES

EFFECTIVE VALUES

EFFECTIVE DIFFUSIVITY

When diffusion varies across the thickness of the layer the exact calculation can be done using the following effective diffusivity

$$D_{\text{eff}} = \left[\frac{1}{y_{\text{B}} - y_{\text{A}}} \int_{y_{\text{A}}}^{y_{\text{B}}} \frac{dy}{D(y)}\right]^{-1} \tag{84}$$

where y is the direction perpendicular to the layer, and y_{A} and y_{B} are the coordinates of each face of the layer.

The dependence of diffusivity on space is typically a dependence of diffusivity with temperature, with temperature depending on space. If the temperature across a layer profile is linear (i.e. the temperature gradient is constant, such as diffusivity within a thermal boundary layer at the surface of molten metal), the effective diffusivity can be expressed as

$$D_{\text{eff}} = \left[\frac{1}{T_{\text{B}} - T_{\text{A}}} \int_{T_{\text{A}}}^{T_{\text{B}}} \frac{dT}{D(T)}\right]^{-1} \tag{85}$$

where T_{A} and T_{B} are the temperatures of each face of the layer. Because in molten metals and in gases the diffusion boundary layer is typically comparable or thinner than the thermal boundary layer, the temperature gradient in the diffusion boundary layer can be considered approximately linear, making Equation 85 applicable.

EFFECTIVE KINEMATIC VISCOSITY

For flow of constant density between parallel plates an exact effective value of effective kinematic viscosity is

$$\nu_{\text{eff}} = \left[\frac{1}{y_{\text{B}} - y_{\text{A}}} \int_{y_{\text{A}}}^{y_{\text{B}}} \frac{dy}{\nu(y)}\right]^{-1} \tag{86}$$

where y is the direction perpendicular to the plates, and y_{A} and y_{B} are the coordinates of each face of the plates.

The dependence of kinematic viscosity on space is typically a dependence with temperature, where temperature depends on space. If the temperature profile between the layers is linear (i.e. the temperature gradient is constant, such as kinematic viscosity within a thermal boundary layer of molten metal at the melting front), the effective kinematic viscosity can be expressed as

$$\nu_{\text{eff}} = \left[\frac{1}{T_{\text{B}} - T_{\text{A}}} \int_{T_{\text{A}}}^{T_{\text{B}}} \frac{dT}{\nu(T)}\right]^{-1} \tag{87}$$

where T_{A} and T_{B} are the temperatures of each face of the plates. Of course, welding seldom involves parallel plates, but the proposed effective kinematic viscosity can be used as an approximation in other cases too. if the magnitude in question were viscosity, an effective viscosity can be estimated with the same approach.

TRANSPORT PROPERTIES OF MOLTEN METALS

The temperatures of molten metal during welding can approach boiling, which is above the range in which measurements were made and correlations developed. In the absence of better data, the values of properties at high temperatures are extrapolated assuming the standard correlations still hold.

DIFFUSIVITY

In molten and solid metal, the diffusivity is captured well with an Arrhenius expression:

$$D(T) = D_0 \exp\left(-\frac{Q}{RT}\right) \tag{88}$$

where Q is the activation energy, R the universal gas constant, and D_0 is a kinetic constant, tabulated for molten steel and molten aluminum in Table 10.

Table 10 Constants for diffusion in molten metals. Calculated values of diffusivity in Fe and Al added for reference

	Solvent	Solute	D_0 $m^2 s^{-1}$	Q kJ mol^{-1}	Source	D $m^2 s^{-1}$
	pure Fe	Si	$5.0\ 10^{-8}$	42.7		$6.80\ 10^{-9}$
	C-saturated Fe	Si	$2.4\ 10^{-8}$	34.3		$4.84\ 10^{-9}$
	pure Fe	S	$4.8\ 10^{-8}$	36.0		$8.99\ 10^{-9}$
Fe	C-saturated Fe	S	$2.8\ 10^{-8}$	31.4	[44]	$6.40\ 10^{-9}$
	C-saturated Fe	Mn	$1.9\ 10^{-8}$	24.3		$6.22\ 10^{-9}$
	2.5% C-Fe	Fe	$9.9\ 10^{-7}$	65.7		$4.60\ 10^{-9}$
		Mg	$9.90\ 10^{-5}$	71.6		$2.63\ 10^{-6}$
		Si	$1.34\ 10^{-7}$	30.0		$2.93\ 10^{-8}$
		Ti	$4.29\ 10^{-7}$	36.3		$6.81\ 10^{-8}$
		Cr	$2.53\ 10^{-7}$	32.8		$4.80\ 10^{-8}$
	Al	Mn	$1.93\ 10^{-7}$	31.0	[45]	$4.01\ 10^{-8}$
		Fe	$2.34\ 10^{-7}$	35.0		$3.97\ 10^{-8}$
		Ni	$9.54\ 10^{-8}$	26.0		$2.55\ 10^{-8}$
		Cu	$1.06\ 10^{-7}$	24.0		$3.14\ 10^{-8}$
		Zn	$5.12\ 10^{-8}$	22.2		$1.66\ 10^{-8}$

Reference temperature for diffusivity in Fe is 2300℃, and for Al is 2100℃. Calculated values are extrapolations to temperatures representative of the molten electrode tip in GMAW

VISCOSITY

Viscosity is often approximated as an Arrhenius expression

$$\eta(T) = \eta_0 \exp\left(\frac{Q}{RT}\right) \tag{89}$$

For steel the values used are $\eta_0 = 7.37\ 10^{-5}$ Pa s^{-1} and $Q = 66.74$ kJmol^{-1} [46], for aluminum, the values used are $\eta_0 = 2.57\ 10^{-4}$ Pa s^{-1} and $Q = 13.08$ kJmol^{-1}[44]. Temperature-dependent kinematic viscosity values are obtained from the ratio

$$\nu(T) = \frac{\eta(T)}{\rho(T)} \tag{90}$$

DENSITY

Density is often approximated with a linear expression.

$$\rho(T) = \rho_0 - A(T - T_0) \tag{91}$$

For steel the values used are $\rho_0 = 7057$ kg m^{-3}at $T_0 = 1550$ and $A = 2.14$ kg m^{-3}K^{-1} [46], for aluminum, the values used are $\rho_0 = 2380$ kg m^{-3}at $T_0 = 660$ and $A = 0.35$ kg m^{-3}K^{-1} [48]

DIFFUSIVITY OF GASES

In gases and metal vapors, the standard kinetic theory of gases is not accurate enough to capture diffusivity well [27], but the Chapman-Enskog theory provides useful estimates [49]. Using this theory, the diffusivity of gas *j* in gas *i* is

$$D_{j,j} = \frac{AT^{312}}{p\sigma_{i,j}^2 \Omega_j M_{ij}^{1/2}} \tag{92}$$

where $D_{i,j}$ is in cm s^{-2}, A is a universal constant equal to 2.66 10^{-3}, p is the gas pressure in bar (usually atmospheric), and $\sigma_{i,j}$ is the effective cross section of atoms in Å.

$$\sigma_{i,j} = \frac{\sigma_i + \sigma_j}{2} \tag{93}$$

with the cross sections tabulated for many components in Table 11. The effective molar weight $M_{i,j}$ in $g\ mol^{-1}$ is calculated as

$$M_{i,j} = 2\left(\frac{1}{M_i} + \frac{1}{M_j}\right)^{-1} \tag{94}$$

and the collision integral Ω_j has the following general expression [50]:

$$\Omega_j = \frac{1.06036}{T_j^{*0.15610}} + \frac{0.193}{\exp(0.47635\, T_j^*)} + \frac{1.03587}{\exp(1.52996\, T_j^*)} + \frac{1.76474}{\exp(3.89411\, T_j^*)} \tag{95}$$

The value of T_j^* is provided by [19] as

$$T_j^* = \frac{kT}{\varepsilon_{i,j}} \tag{96}$$

$$\varepsilon_{i,\,j} = \sqrt{\varepsilon_i \varepsilon_j} \tag{97}$$

where T is the temperature of the gas, and the Lennard-Jones energies ε are tabulated in Table 11.

VAPOR PRESSURE OF MOLTEN METALS

The vapor pressure of the component is typically tabulated as [53]:

$$\log p_{\mathrm{lg}_j} = \mathrm{A} + \mathrm{B}T^{-1} + \mathrm{C}\log T + \mathrm{D}T^{-3} \tag{98}$$

where p_{lg_j} is in atm, and the values of A, B, C, D listed in Table 12.

COMPOSITION OF MIXTURES

The molar fraction of component i (X_i) and mass fraction of component i are related as

$$X_i = \frac{f_i M}{M_i} \tag{99}$$

where M_i is the molar mass of component i, and M is the overall molar mass of the mixture:

$$\mathrm{M} = \left(\sum_i \frac{f_i}{M_i} \right)^{-1} \tag{100}$$

$$\mathrm{M} = \sum_i X_i M_i \tag{101}$$

Table 11 Chapman-Enskog constants for gas diffusion. Calculated values of diffusion in Ar at 5000K added for reference

	Element	σ Å	ε 10^{-20}J	Source	$D_{Ar,j}$@ 5000K $10^{-3}m^2s^{-1}$
Shielding gas	He	2.55	0.0141	[51]	-
	CO_2	3.94	0.269		-
	Ar	3.54	0.129		-
Metal vapor	Li	2.98	2.52	[52]	3.53
	Na	3.66	1.83		1.89
	Mg	3.18	2.18		2.10
	Al	2.76	3.70		2.22
	Si*	2.86	5.62		2.05
	K	4.54	1.64		1.30
	Mn*	2.58	3.71		1.96
	Fe	2.47	4.93		1.98
	Co	2.43	5.00		1.98
	Ni	2.43	4.90		1.99
	Cu	2.44	4.51		1.96
	Zn	2.51	1.87		2.05
	Ga	2.80	3.58		1.75
	Ag	2.74	3.87		1.65
	Cd	2.97	1.65		1.64
	In	3.16	3.75		1.45
	Sn	3.25	4.83		1.37
	Sb	3.18	2.72		1.46
	Pb	3.29	3.16		1.33
	Hg	2.92	1.00		1.63
	Tl	3.19	2.75		1.71
	Bi	3.37	2.78		1.31
	Pu	3.11	5.67		1.32

Estimated error of these parameters is $\pm$10% [19].

Table 12 Constants for vapor pressure of liquid metals

Element	A	B	C	D
Li	5.055	-8023		
Na	4.704	-5377		
Mg ‡	4.89	-6685.1		
Al	5.911	-16211		
Si §	5.84	-20800		
Ti	6.358	-22747		
Cr	6.8	-20733	0.4391	-0.4094
Mn †	4.94	-11542		
Fe	6.347	-19574		
Ni	6.666	-20765		
Cu	5.849	-16415		
Zn	5.378	-6286		
Ag	5.752	-13827		
Pt	6.386	-26856		

All values from [53], except ‡ from boiling temperature and enthalpy, § from [54], and † from boiling temperature and enthalpy in [55]. Estimated error of these parameters is ±5% [53].